Journal of Sound and Vibration (2001) **240**(5), 789–808
doi:10.1006/jsvi.2000.3195, available online at http://www.idealibrary.com on IDEAL®

A STUDY ON THE SQUEAL OF A DRUM BRAKE WHICH HAS SHOES OF NON-UNIFORM CROSS-SECTION

J. M. LEE

School of Mechanical and Aerospace Engineering, Seoul National University, San 56-1, *Shinrim-dong, Kwanak-ku, Seoul* 151-742, *Korea. E-mail: leejm@gong.snu.ac.kr*

S. W. YOO

Turbo and Power Machinery Research Center (TPMRC), Seoul National University, San 56-1, *Shinrim-dong, Kwanak-ku, Seoul* 151-742. *Korea, E-mail: sungwoo@ryu.snu.ac.kr*

J. H. KIM

Institute of Advanced Machinery and Design, Seoul National University, San 56-1, *Shinrim-dong, Kwanak-ku, Seoul* 151-742, *Korea*

AND

C. G. AHN

Research Institute of Engineering Science, Seoul National University, San 56-1, *Shinrim-dong, Kwanak-ku, Seoul* 151-742, *Korea*

(*Received* 19 *October* 1999, *and in final form* 25 *April* 2000)

A stability analysis of a drum brake, which has shoes of *non-uniform cross-section*, is performed to find a simple and effective method of reducing the squeal of the drum brake by partially changing the shapes of the shoes. The squeal is considered as a noise induced by the self-excited vibration of the drum brake which makes the brake unstable. Shoes of *non-uniform cross-section* are often used for the drum brake of current passenger cars to reduce the squeal. However, the influence of this non-uniformity upon the squeal has not been analyzed theoretically. In this study, the drum and the shoes are assumed as a uniform ring and non-uniform arches, respectively, for modelling the brake. For a reasonable method of modelling, the vibration characteristics of the brake and their relations to the squeal are discussed based on the results of modal tests. The influences of brake design parameters upon the squeal are investigated, and a minor change of the cross-section is proposed to reduce the squeal. The effect of the minor change is verified through noise dynamometer tests. In addition, the effect of asymmetry of the drum, which can be built by mass addition, is presented.

© 2001 Academic Press

1. INTRODUCTION

Squeal is a significant noise problem occurring in vehicle braking systems, mass transit systems, etc. Kootwijk-Damman [1] and Nakai *et al.* [2] have been investigated railway wheel squeal of mass transit systems, and McMillan [3] has developed a non-linear friction model for the understanding of the phenomenon of railway wheel squeal. Many studies on the squeal of vehicle braking systems have also been performed since the 1920s.

Earlier studies on the brake squeal focused on "stick–slip" caused by the coefficient of static friction, higher than that of dynamic friction. Subsequently, negative friction–velocity

0022-460X/01/100789 + 20 $35.00/0 © 2001 Academic Press

slope as well as "sprag-slip" phenomenon was considered as a reason of the squeal [4–8]. Millner introduced an idea that the squeal is a phenomenon of dynamic instability caused by the coupling effects between brake components; the coupling effects are built by the frictional force variations due to the variation in normal forces between the brake components [9]. He proposed a new theoretical model of a drum brake, and Okamura *et al.* improved his model to represent a real drum brake in more detail [10]. The study on the squeal has been continued by Lang *et al*, Chen *et al*., Zhu *et al*., Hultén and so forth [11–17]. Hultén proposed a model of a drum brake in which the drum and the shoes were assumed to be distributed mass-spring systems. In these studies, the squeal of drum brakes which have shoes of *uniform cross-section* has been investigated.

Shoes of *non-uniform cross-section* are often used for the drum brake of recent passenger cars to reduce the squeal. The *non-uniform cross-section* is built by changing the shapes of the shoes partially, and this minor change is a simple and effective method to reduce the squeal. However the method of changing the shapes has not as yet been analyzed theoretically, but determined through perception and experiment.

This paper deals with a theoretical analysis for the squeal of a drum brake which has the shoes of *non-uniform cross-section.* A minor change of the shoe's cross-section will be proposed to reduce the squeal, and the effect of the change will be verified through noise dynamometer tests. In addition, the effect of mass addition to the drum, which was investigated by Lang *et al.* [18] through a simple binary flutter model, will be presented.

2. EXPERIMENTAL INVESTIGATION FOR THE DYNAMIC CHARACTERISTICS OF THE DRUM BRAKE

The squeal was monitored during drive tests of a passenger car and measured to have frequencies of 3·1 and 5·1 kHz; the 3·1 kHz squeal will be mainly dealt with in this paper. The squeal is a complex phenomenon caused by the dynamic behavior of the brake parts and friction mechanism. In this section, the effects of the dynamic characteristics of the drum and the shoes are to be discussed. Modal tests were performed to investigate the dynamic characteristics. From the results of the modal tests, it was found that the dynamic characteristics of the brake parts vary as they are assembled and the brake pressure is applied. Therefore, the experimental investigations will be focused on the comparison of the brake parts in freely supported condition with the brake assembly to which the brake pressure is applied.

2.1. DYNAMIC CHARACTERISTICS OF THE BRAKE PARTS

The modal parameters of the drum and the shoe, not assembled together, were estimated through the modal tests. Figure 1 is the photo of the drum and the shoe used in this study, and the points of FRF acquisition during the modal tests are shown. The shoe consists of the web and the rim; the web is attached to the rim to increase the stiffness of the shoe. The number of the FRF acquisition during the modal tests are shown. The shoe consists of the web and the rim; the web is attached to the rim to increase the stiffness of the shoe. The number of the FRF acquisition points of the drum and the shoe are 20 and 8 respectively.

Table 1 shows the natural frequencies of the drum and the shoe in freely supported condition extracted from the modal tests, and the mode shapes of mode Nos. 2d and 2s are represented in Figure 2. Because mode No. 2d has two natural frequencies as a pair, only one mode shape is shown in Figure 2(a); another mode shape is identical with that in

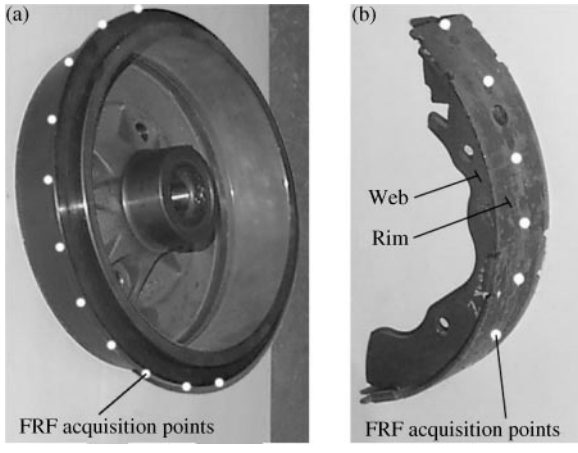

Figure 1. Photo of (a) the drum and (b) the shoe.

TABLE 1

Natural frequencies of the drum and the shoe extracted from the modal tests performed in freely supported condition

Component	Mode no.	Natural frequency (kHz)
Drum	1d	1·07, 1·10
	2d	2·62, 2·70
	3d	4·79
Shoe	1s	2·11
	2s	5·56
	3s	7·29

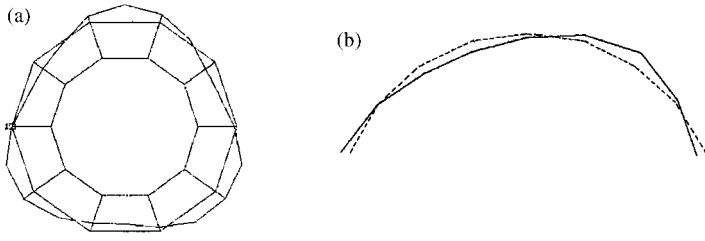

Figure 2. Mode shapes of the drum and the shoe extracted from the modal test performed in freely supported condition: (a) mode No. 2d of the drum; (b) mode No. 2s of the shoe.

Figure 2(a) except the positions of nodes and anti-nodes. As shown in Figure 2, the mode shape of mode No. 2d closely resembles the second flexural mode shape of a freely supported ring, and the mode shape of mode No. 2s also resembles the second bending mode shape of a freely supported arch.

2.2. DYNAMIC CHARACTERISTICS OF THE DRUM BRAKE ASSEMBLY

The modal tests for the drum brake assembly were also performed under the condition of 32 bar brake pressure. Figure 3 shows the drum brake assembly; the lining is attached to the

shoe and the friction is occurred between the lining and the drum. The number of the FRF acquisition points of the drum and the shoe are 20 and 16 (8 at each end of the rim) respectively.

Table 2 shows the natural frequencies of the drum brake assembly which are close to the frequencies of the squeal measured from the drive tests, and the mode shapes of mode No. 2a related to the 3·1 kHz squeal are represented in Figure 4. The circle and the circular strip represent the drum and the shoe, respectively, in this figure. The mark X means the same position in the circumferential direction and only one shoe in the assembly is represented. In this figure, the drum of mode No. 2a has the mode shapes almost identical with the mode shape of mode No. 2d in Figure 2(a); the drum almost keeps the mode shapes of freely supported state when the shoe is coupled up to the drum and the brake pressure is applied. Therefore, the mode shapes of freely supported drum can be used in theoretical analysis. However, it is difficult to say that the shoe also keeps the mode shapes of freely supported state when the brake pressure is applied. As shown in Figure 4, the mode shapes of the shoe vary according to those of the drum.

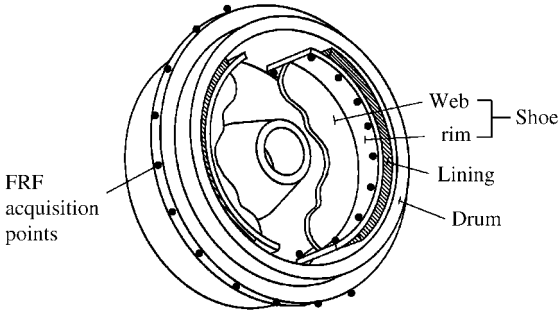

Figure 3. Figure of the drum brake assembly.

TABLE 2

Natural frequencies of the drum brake assembly extracted from the modal tests and the squeal frequencies measured from the drive tests

Mode no.	Natural frequency from modal test (kHz)	Squeal frequency measured from the drive tests (kHz)
2a	2·90, 3·18	3·1
3a	5·03	5·1

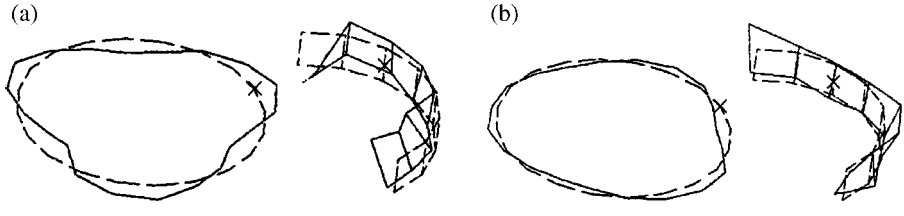

Figure 4. Mode shapes of mode No. 2a (brake assembly) related to the 3·1 kHz squeal extracted from the modal test: (a) 2·90 kHz; (b) 3·18 kHz.

As shown in Table 1, the natural frequencies of the drum are quite close to the squeal frequencies in comparison with the shoe; the squeal frequencies are a little higher than the natural frequencies of the freely supported drum because of the brake pressure. This means that the vibration characteristics of the drum changes just a little when the brake pressure is applied, while those of the shoe changes very much.

2.3. MODE SHAPES OF THE DRUM AND THE SHOE USED IN ANALYSIS

Millner and Okamura *et al.* used the natural mode shapes of the freely supported ring and arch in their model, and they assumed that the mode shapes of mode No. 2a consist of those of mode Nos. 2d and 2s [9, 10]. It is possible to assume that the mode shapes of the drum in mode No. 2a are the same as the mode shapes of mode No. 2d, that is, the 2nd flexural mode shape of a freely supported ring. However, the mode shapes of the shoe in mode No. 2a are not identical with the mode shape of mode No. 2s, that is, the 2nd bending mode shape of a freely supported arch. The mode shapes of the shoe in the brake assembly are dependent on the behavior of the drum. Therefore, series of trial functions will be used to approximate the mode shapes of the shoes in this paper. Moreover, the *non-uniform and arbitrary cross-section* of the shoe makes it necessary to use approximate method to the shoes.

3. THEORETICAL MODEL

Figure 5 shows a dynamic model of the brake assembly. The drum and the shoes were regarded as a uniform thin ring and non-uniform thin arches respectively. Therefore, the model was built considering the radial and circumferential displacements of the brake components. The drum and the shoes can be regarded as a thick ring and thick arches, respectively, and then shear deformation and rotary inertia must be considered by adding a rotational degree of freedom to the model. However, the squeal was analyzed as

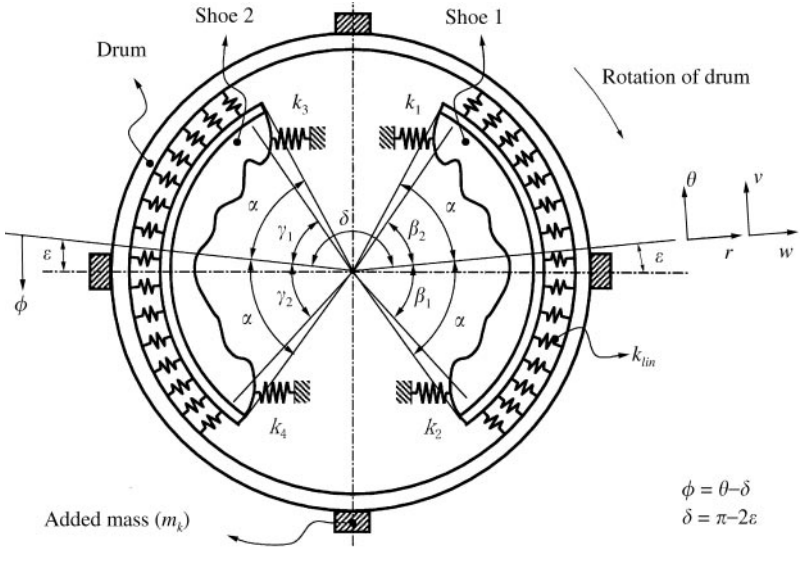

Figure 5. Theoretical model of a drum brake assembly.

a phenomenon of dynamic instability caused by the frictional force variations due to the variation in normal forces between the brake components, and the normal forces are caused by the radial displacement; the radial displacement is coupled with the circumferential displacement in thin ring theory. Therefore, the effect of the rotational degree of freedom is much less than that of the radial and the circumferential displacements, and thin ring theory was used in this analysis. The dynamic characteristics of the thin ring and arches come to be identical with those of the drum and shoes, by calculating the parameters of the thin ring and arches according to the procedures represented in section 5.

Parameters w and v are the radial and the circumferential displacements, and they are subdivided by the subscripts d, 1 and 2; w_d and v_d are the displacements of the drum, and w_1, v_1, w_2 and v_2 are those of shoes 1 and 2. The circumferential co-ordinates θ and ϕ have their origins at the center of shoes 1 and 2, respectively, and δ is the angular distance between their origins. Parameters β_1 and β_2 are the angular distances between the center of shoe 1 and the ends of the lining attached to shoe 1. In the case of shoe 2, γ_1 and γ_2 are used instead of β_1 and β_2. The linings were modelled as distributed radial springs. The spring constants k_1, k_2, k_3 and k_4 are equivalent to the normal components of contact stiffnesses. The tangential components are neglected because they are very small due to lubricating the contact surfaces with grease. The kth lumped mass attached to the drum to analyze the effects of asymmetry is stated as m_k. The asymmetry of a ring oppresses the wave motions by fixing its mode shapes to its body, so it results in the decrease of instability. The effects of drum rotation were neglected with the exception of the frictional forces between the drum and the lining, because the rotation speed was much less than the vibration speed of the drum.

4. EQUATION OF MOTION

4.1. KINETIC AND POTENTIAL ENERGIES

The equation of motion was obtained by the assumed-modes method. The kinetic and the potential energies of the drum brake were calculated as

$$K = K_d + K_s, \qquad U = U_d + U_s + U_{lin} + U_k, \tag{1a, b}$$

where K and U are the kinetic and the potential energies, and the subscripts d, s, lin and k mean the drum (the ring), the shoe (the arch), the lining and the contact stiffness respectively.

The kinetic and the potential energies of the ring are given by the expressions

$$K_d = \frac{1}{2}\rho_d A_d r_d \int_0^{2\pi} \left\{ \left(\frac{\partial^2 v_d}{\partial t \partial \theta} \right)^2 + \left(\frac{\partial v_d}{\partial t} \right)^2 \right\} \mathrm{d}\theta + \sum_{k=1}^{r} \int_0^{2\pi} \left[\frac{1}{2} m_k \left\{ \left(\frac{\partial^2 v_d}{\partial t \partial \theta} \right)^2 + \left(\frac{\partial v_d}{\partial t} \right)^2 \right\} \delta(\theta - \theta_k) \right] \mathrm{d}\theta, \tag{2}$$

$$U_d = \frac{EI_d}{2r_d^3} \int_0^{2\pi} \left(\frac{\partial v_d}{\partial \theta} + \frac{\partial^3 v_d}{\partial \theta^3} \right)^2 \mathrm{d}\theta, \tag{3}$$

where ρ_d, A_d, r_d and EI_d are the density, the cross-sectional area, the radius of neutral surface and the bending stiffness of the ring respectively. In equation (2), r is the number of added masses and $\delta(\theta - \theta_k)$ is a Dirac delta function in which θ_k is the angular position of

the added mass m_k. Equations (2) and (3) were derived by applying the inextensional approximation

$$w_d = -\frac{\partial v_d}{\partial \theta}, \tag{4}$$

because the drum had almost identical flexural mode shapes with those of a freely supported ring.

The inextensional approximation cannot be applied to the arches because of the contact stiffnesses at the ends. Therefore, the kinetic and the potential energies of the arches are given by the expressions

$$K_s = \frac{1}{2}\rho_1 \int_{-\alpha}^{\alpha} A_1(\theta) r_1(\theta) \left\{ \left(\frac{\partial w_1}{\partial t}\right)^2 + \left(\frac{\partial v_1}{\partial t}\right)^2 \right\} \mathrm{d}\theta + \frac{1}{2}\rho_2 \int_{-\alpha}^{\alpha} A_2(\phi) r_2(\phi) \left\{ \left(\frac{\partial w_2}{\partial t}\right)^2 + \left(\frac{\partial v_2}{\partial t}\right)^2 \right\} \mathrm{d}\phi, \tag{5}$$

$$U_s = \frac{E_1}{2} \int_{-\alpha}^{\alpha} \left\{ \frac{I_1(\theta)}{r_1^3(\theta)} \left(\frac{\partial v_1}{\partial \theta} - \frac{\partial^2 w_1}{\partial \theta^2}\right)^2 + \frac{A_1(\theta)}{r_1(\theta)} \left(\frac{\partial v_1}{\partial \theta} + w_1\right)^2 \right\} \mathrm{d}\theta + \frac{E_2}{2} \int_{-\alpha}^{\alpha} \left\{ \frac{I_2(\phi)}{r_2^3(\phi)} \left(\frac{\partial v_2}{\partial \phi} - \frac{\partial^2 w_2}{\partial \phi^2}\right)^2 + \frac{A_2(\phi)}{r_2(\phi)} \left(\frac{\partial v_2}{\partial \phi} + w_2\right)^2 \right\} \mathrm{d}\phi, \tag{6}$$

where ρ_1, A_1, r_1, E_1 and I_1 are the density, the cross-sectional area, the radius of neutral surface, the Young's modulus and the cross-sectional moment of inertia of the arch equivalent to shoe 1, respectively; and ρ_2, A_2, r_2, E_2 and I_2 are those of the arch equivalent to shoe 2. By approximating the profile of the web to spline functions, A_1, A_2, r_1, r_2, I_1 and I_2 are obtained as functions of θ or ϕ, then the integration in equations (5) and (6) can be performed. Figure 6 represents the profile of the web obtained by the spline functions used in this analysis.

The potential energy of the lining can be derived from the relative displacements of the ring and the arches as

$$U_{lin} = \frac{1}{2} k_{lin} \left[\int_{-\beta_1}^{\beta_2} \left(w_1 + \frac{\partial v_d}{\partial \theta} \right)^2 \mathrm{d}\theta + \int_{-\gamma_1}^{\gamma_2} \left(w_2 + \frac{\partial v_d}{\partial \theta} \right)^2 \mathrm{d}\phi \right], \tag{7}$$

where the radial spring constant of the lining per unit angle

$$k_{lin} = \frac{E_{lin} b_{lin} r_{lin}}{h_{lin}}. \tag{8}$$

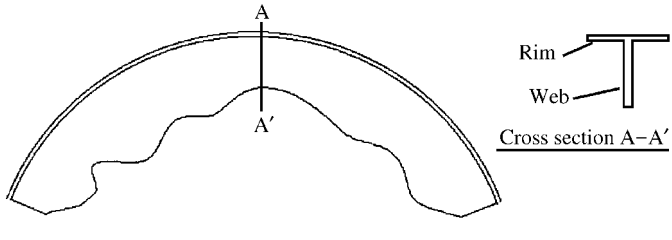

Figure 6. Web profile of the original shoe obtained by spline functions and the cross-section of the shoe.

E_{lin}, b_{lin}, r_{lin} and h_{lin} are the Young's modulus, the width, the radius and the thickness of the lining. The potential energy due to the contact stiffnesses at the ends of the arches

$$U_k = \frac{1}{2}k_1\int_{-\alpha}^{\alpha}\{w_1\cos(\alpha+\varepsilon) - v_1\sin(\alpha+\varepsilon)\}^2\delta(\theta-\alpha)\,\mathrm{d}\theta + \frac{1}{2}k_2\int_{-\alpha}^{\alpha}\{w_1\cos(\alpha-\varepsilon) + v_1\sin(\alpha-\varepsilon)\}^2\delta(\theta+\alpha)\,\mathrm{d}\theta + \frac{1}{2}k_3\int_{-\alpha}^{\alpha}\{w_2\cos(\alpha+\varepsilon) + v_2\sin(\alpha+\varepsilon)\}^2\delta(\theta+\alpha)\,\mathrm{d}\phi + \frac{1}{2}k_4\int_{-\alpha}^{\alpha}\{w_2\cos(\alpha-\varepsilon) - v_2\sin(\alpha-\varepsilon)\}^2\delta(\theta-\alpha)\,\mathrm{d}\phi, \tag{9}$$

where $\delta(\theta-\alpha)$ and $\delta(\theta+\alpha)$ are Dirac delta functions.

4.2. MODE SHAPES OF THE RING AND THE ARCHES

The squeal of 3·1 kHz was analyzed in this study, so a pair of second flexural modes of the ring was used. The mode shapes of the arches were approximated by a series of trial functions, because the arches have non-uniform cross-sections and are assembled with the ring equivalent to the stiff and massive drum. This means that approximate method was partially used by considering a series of trial functions for the arches only.

The circumferential displacement of the ring

$$v_d = \cos n\theta\eta_1(t) + \sin n\theta\eta_2(t), \tag{10}$$

where $\eta_1(t)$ and $\eta_2(t)$ are the generalized co-ordinates of a pair of ring modes, and the constant n is the number of nodal lines; for example, the n of the second flexural mode is 3. By including only a pair of the ring modes, the squeal of a specific frequency can be analyzed separately. The radial displacement of the ring is calculated from equations (4) and (10).

Polynomials are used for the trial functions of arches as

$$w_1 = \sum_{j=1}^{N}\theta^{j-1}\zeta_{1j}(t), \qquad v_1 = \sum_{j=1}^{N}\theta^{j-1}\xi_{1j}(t), \tag{11a, b}$$

$$w_2 = \sum_{j=1}^{N}\phi^{j-1}\zeta_{2j}(t), \qquad v_2 = \sum_{j=1}^{N}\phi^{j-1}\xi_{2j}(t), \tag{12a, b}$$

where N is the number of trial functions and $\zeta_{1j}(t)$, $\xi_{1j}(t)$, $\zeta_{2j}(t)$ and $\xi_{2j}(t)$ are the generalized co-ordinates of those functions.

4.3. GENERALIZED FORCES DUE TO FRICTION

The frictional forces applied on the arches are obtained from the relative displacements of the ring and the arches as

$$F_1 = -\mu k_{lin}\left(w_1 + \frac{\partial v_d}{\partial\theta}\right), \qquad F_2 = -\mu k_{lin}\left(w_2 + \frac{\partial v_d}{\partial\theta}\right), \tag{13a, b}$$

where μ is the coefficient of friction of the lining. The frictional forces equal in magnitude and opposite in direction are applied on the ring. The generalized forces due to the frictional forces applied on the arches are given by the expressions

$$Q_{1i} = \int_{-\beta_1}^{\beta_2} F_1 \frac{\partial v_1}{\partial \xi_{1i}} \, \mathrm{d}\theta, \qquad Q_{2i} = \int_{-\gamma_1}^{\gamma_2} F_2 \frac{\partial v_2}{\partial \xi_{2i}} \, \mathrm{d}\phi, \quad \text{where } i = 1, 2, \ldots, N. \tag{14a, b}$$

In the case of the ring, the generalized forces

$$Q_{di} = -\int_{-\beta_1}^{\beta_2} F_1 \frac{\partial v_d}{\partial \eta_i} \, \mathrm{d}\theta - \int_{-\gamma_1}^{\gamma_2} F_2 \frac{\partial v_d}{\partial \eta_i} \, \mathrm{d}\phi, \quad \text{where } i = 1, 2. \tag{15}$$

4.4. EQUATION OF MOTION

By substituting equations (1)–(15) into Lagrange's equation, the equations of motion of the drum brake with friction are obtained as

$$c_1\ddot{\eta}_1 + c_3\ddot{\eta}_2 + (c_4 + k_{lin}n^2c_5 + \tfrac{1}{2}\mu k_{lin}nc_6)\eta_1 - (\tfrac{1}{2}k_{lin}n^2c_6 + \mu k_{lin}nc_7)\eta_2 - \sum_{j=1}^{N} [(k_{lin}nc_{8j} + \mu k_{lin}c_{9j})\zeta_{1j} + (k_{lin}nc_{10j} + \mu k_{lin}c_{11j})\zeta_{2j}] = 0, \tag{16a}$$

$$c_3\ddot{\eta}_1 + c_2\ddot{\eta}_2 + (-\tfrac{1}{2}k_{lin}n^2c_6 + \mu k_{lin}nc_5)\eta_1 + (c_4 + k_{lin}n^2c_7 - \tfrac{1}{2}\mu k_{lin}nc_6)\eta_2 + \sum_{j=1}^{N} [(k_{lin}nc_{9j} - \mu k_{lin}c_{8j})\zeta_{1j} + (k_{lin}nc_{11j} - \mu k_{lin}c_{10j})\zeta_{2j}] = 0, \tag{16b}$$

$$\sum_{j=1}^{N} [c_{12}\ddot{\zeta}_{1j}] - k_{lin}nc_{8i}\eta_1 + k_{lin}nc_{9i}\eta_2 + \sum_{j=1}^{N} [(c_{18} + k_{lin}c_{22} + c_{28})\zeta_{1j} + (c_{16} + \tfrac{1}{2}c_{24})\xi_{1j}] = 0, \tag{16c}$$

$$\sum_{j=1}^{N} [c_{12}\ddot{\xi}_{1j}] - \mu k_{lin}nc_{8i}\eta_1 + \mu k_{lin}nc_{9i}\eta_2 + \sum_{j=1}^{N} [(c_{14} + \tfrac{1}{2}c_{24} + \mu k_{lin}c_{22})\zeta_{1j} + (c_{20} + c_{26})\xi_{1j}] = 0, \tag{16d}$$

$$\sum_{j=1}^{N} [c_{13}\ddot{\zeta}_{2j}] - k_{lin}nc_{10i}\eta_1 + k_{lin}nc_{11i}\eta_2 + \sum_{j=1}^{N} [(c_{19} + k_{lin}c_{23} + c_{29})\zeta_{2j} + (c_{17} + \tfrac{1}{2}c_{25})\xi_{2j}] = 0, \tag{16e}$$

$$\sum_{j=1}^{N} [c_{13}\ddot{\xi}_{2j}] - \mu k_{lin}nc_{10i}\eta_1 + \mu k_{lin}nc_{11i}\eta_2 + \sum_{j=1}^{N} [(c_{15} + \tfrac{1}{2}c_{25} + \mu k_{lin}c_{23})\zeta_{2j} + (c_{21} + c_{27})\xi_{2j}] = 0, \tag{16f}$$

where i is an integer between 1 and N; the integer i is the subscript of c_{8i}, c_{9i}, c_{10i} or c_{11i} in equations (16c)–(16f). Therefore, each equation in equations (16c)–(16f) can be expanded to N equations; the total number of equations is $4N + 2$. The coefficients (c_1–c_{29}) are represented in Appendix A. These equations of motion can be rearranged to a matrix form as

$$\mathbf{M}\ddot{\mathbf{x}} + \mathbf{K}\mathbf{x} = 0, \tag{17}$$

where $\mathbf{x} = \{\eta_1\ \eta_2\ \zeta_{11} \cdots \zeta_{1N}\ \xi_{11} \cdots \xi_{1N}\ \zeta_{21} \cdots \zeta_{2N}\ \xi_{21} \cdots \xi_{2N}\}^{\mathrm{T}}$,

$$\mathbf{M} = \begin{bmatrix} \mathbf{M}_{11} & \mathbf{0} & \mathbf{0} & \mathbf{0} & \mathbf{0} \\ \mathbf{0} & \mathbf{M}_{22} & \mathbf{0} & \mathbf{0} & \mathbf{0} \\ \mathbf{0} & \mathbf{0} & \mathbf{M}_{33} & \mathbf{0} & \mathbf{0} \\ \mathbf{0} & \mathbf{0} & \mathbf{0} & \mathbf{M}_{44} & \mathbf{0} \\ \mathbf{0} & \mathbf{0} & \mathbf{0} & \mathbf{0} & \mathbf{M}_{55} \end{bmatrix}, \quad \mathbf{K} = \begin{bmatrix} \mathbf{K}_{11} & \mathbf{K}_{12} & \mathbf{0} & \mathbf{K}_{14} & \mathbf{0} \\ \mathbf{K}_{21} & \mathbf{K}_{22} & \mathbf{K}_{23} & \mathbf{0} & \mathbf{0} \\ \mathbf{K}_{31} & \mathbf{K}_{32} & \mathbf{K}_{33} & \mathbf{0} & \mathbf{0} \\ \mathbf{K}_{41} & \mathbf{0} & \mathbf{0} & \mathbf{K}_{44} & \mathbf{K}_{45} \\ \mathbf{K}_{51} & \mathbf{0} & \mathbf{0} & \mathbf{K}_{54} & \mathbf{K}_{55} \end{bmatrix}.$$

$\mathbf{M}$ and $\mathbf{K}$ are $(4N + 2)$ by $(4N + 2)$ matrices; sub-matrices $\mathbf{M}_{11}$ and $\mathbf{K}_{11}$ are 2×2 and the other sub-matrices diagonal in $\mathbf{M}$ and $\mathbf{K}$ are $N \times N$. The components of the sub-matrices are represented in Appendix B.

The dynamic stability of the brake system can be determined by the real parts of the eigenvalues obtained from equation (17). The matrices $\mathbf{M}$ and $\mathbf{K}$ are symmetric when the coefficient of friction μ is zero, but $\mathbf{K}$ becomes asymmetric as μ is not equal to zero. The asymmetry of $\mathbf{K}$ can induce the positive real parts which result in the negative damping ratios of the system; the negative damping ratios make the vibration of the system diverge. Therefore, the system comes to have the instability that results in the generation of the squeal.

5. EQUIVALENT PARAMETERS

The simulation for the squeal of 3·1 kHz is performed in this study, by including only a pair of the 2nd flexural modes of the ring. Therefore, the equivalent parameters of the drum brake associated with the squeal of 3·1 kHz are presented in this paper.

The cross-sectional area and the bending stiffness of the ring are different from those of the drum which are directly calculated from the cross-sectional dimensions of the drum. The two parameters of the ring should be calculated as equivalent parameters which represent the modal characteristics of the drum. However, the two equivalent parameters cannot be obtained simultaneously. After one of the two is determined, another parameter will be obtained if the natural frequency of the ring is known. This is because the cross-sectional area and the bending stiffness are applied to the kinetic and the potential energies, respectively, and then the natural frequency is determined from both of the kinetic and the potential energies. Accordingly, the equivalent parameters of the ring are obtained from the following procedure.

(i) Calculate the reference kinetic energy of the drum by FE analysis; the reference kinetic energy does not include the natural frequencies of the drum. The reference kinetic energy is used instead of the kinetic energy, because the natural frequencies of the drum calculated by FE analysis is not exactly equal to those of the real drum. Figure 7(a) represents mode No. 2d used in the calculation of the reference kinetic energy.

(ii) Calculate the reference kinetic energy of the ring's second flexural mode as a function of cross-sectional area A_d.

(iii) Obtain A_d from the fact that the two reference kinetic energies, calculated from the above procedure, must be of an equal value.

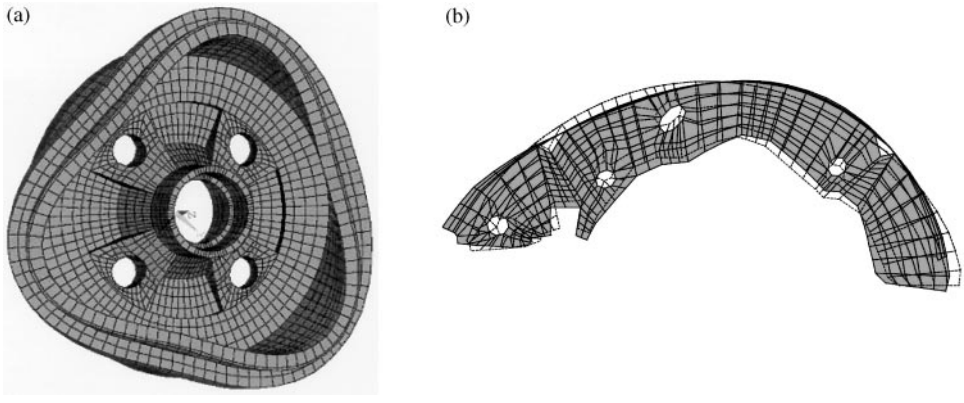

Figure 7. Mode shapes of the drum and the shoe extracted from the FE analysis performed in freely supported condition: (a) mode No. 2d of the drum; (b) mode No. 2s of the shoe.

TABLE 3

Parameters for the analysis of 3·1 *kHz squeal* (*MKS unit*)

Component	Parameter	Value	Parameter	Value
Drum	A_d	$9{\cdot}51 \times 10^{-4}$	r_d	0·1061
	EI_d	4363·2	ρ_d	7250
Shoe	rA	2·87	ρ_1, ρ_2	7850
	rI	1·16	E_1, E_2	210×10^9
Lining	b_{lin}	0·0365	r_{lin}	0·0999
	h_{lin}	0·0035	E_{lin}	$3{\cdot}0 \times 10^7$
Contact stiffness	k_1, k_4	$1{\cdot}0 \times 10^8$	k_2, k_3	$6{\cdot}0 \times 10^8$
Geometry	α	68·5°	β_1	65·5°
	δ	180°	β_2	44·5°

(iv) Calculate the natural frequency of the ring's second flexural mode as a function of bending stiffness EI_d.

(v) Obtain EI_d from the fact that the natural frequencies of the ring and the real drum must be of an equal value. The natural frequency of the real drum is shown in Table 1.

This procedure is also applied to the equivalent parameters of the arches A_1, A_2, I_1 and I_2. However, these parameters cannot be obtained directly from this procedure, because these are not constants but the spline functions. As a result, scale factors rA and rI are introduced; A_1 and A_2 are calculated by multiplying rA to the real cross-sectional areas of the shoes, and I_1 and I_2 by multiplying rI to the real cross-sectional moments of inertia of the shoes. Because the shapes of the two shoes are the same, only the two scale factors are introduced. These scale factors, which determine the equivalent parameters of the arches, can be obtained by applying the above-mentioned procedure. Figure 7(b) shows mode No. 2s used in the calculation of the reference kinetic energy.

This concept of equivalent parameters is also necessary to build a reasonable coupled system of the ring and the arches, because the modal characteristics of the coupled system are determined by the amount of kinetic and potential energies occupied by the ring or the arches in the system. Table 3 shows the parameters of the ring and the arch including the above-mentioned equivalent parameters.

6. RESULTS AND APPLICATION

6.1. RESULTS OF EIGENVALUE ANALYSES

Eigenvalue analyses of equation (17) were performed to determine the dynamic stability of the brake system. Two modes, i.e., a pair of second flexural modes of the ring and two flexural modes for the arches were used in calculation of Figures 8 and 9, because the squeal of 3·1 kHz was analyzed in this study. As stated in section 4.2, ideal ring mode shapes were used for the ring, but approximated mode shapes were used for the arches; 3 was used for n in equation (10) and 20 was used for N in equations (11) and (12). Eighty polynomials were used as the trial functions for the modes shapes of the two arches. Therefore, **M** and **K** in equation (17) were 82×82 matrices.

Figure 8 shows the natural frequencies and the real parts of the eigenvalues obtained by the eigenvalue analyses with variation of the coefficient of friction. As shown in Figure 8(a), the two different lines of the natural frequencies converge at the coefficient of friction of 0·37. This is because the eigenvalues are pure imaginaries not equal in magnitude at the coefficient of friction less than 0·37, and are complex numbers equal in magnitude at the coefficient of friction between 0·37 and 1. The complex numbers have the positive and the negative real parts as shown in Figure 8(b), and the positive real parts make the system unstable. Therefore, the coefficient of friction of 0·37 is a critical value of the squeal. In the unstable region, the system has a complex mode shape because of the complex eigenvalue, therefore the behavior of the system comes to be a wave motion.

Figure 9 shows that the unstable system has the wave motion, while the stable system has the mode shape fixed to its body. The wave motion of the squealing brake was investigated experimentally by Lang *et al.* and Hultén [11, 17]. Consequently, the instability of the system is reduced by oppressing the wave motion. It is also found that the mode shapes of

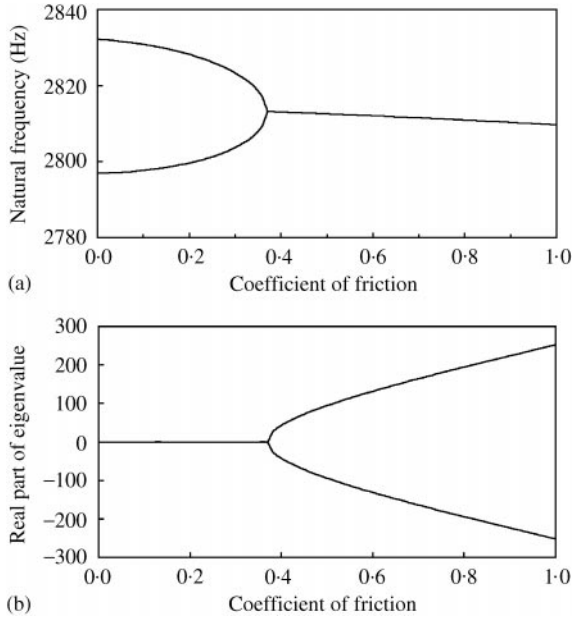

Figure 8. Natural frequencies and real parts of the eigenvalues with variation of the friction coefficient: (a) natural frequencies; (b) real parts of the eigenvalues.

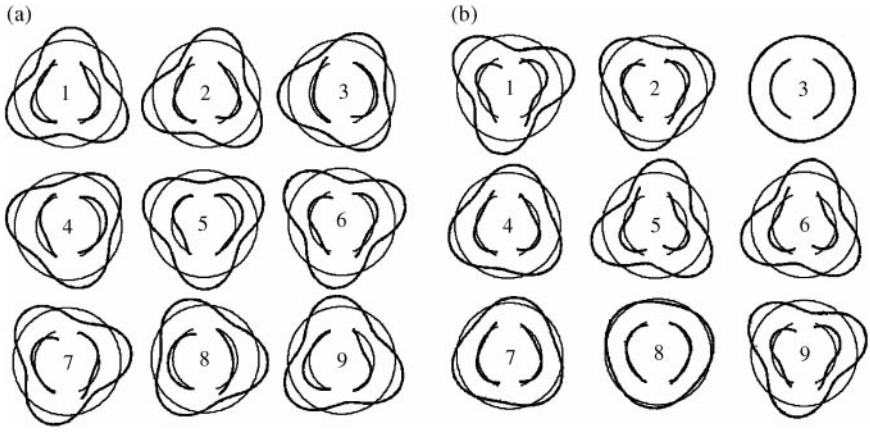

Figure 9. Animated mode shapes of the drum brake: (a) unstable system; (b) stable system. The integers mean the steps of the motion.

the arches in the stable system are not identical with those of freely supported arches, but are dependent on the mode shape of the ring.

6.2. PARAMETER STUDIES AND DISCUSSIONS

The positive real parts of the eigenvalues were calculated with variation of each parameter to find the influences of the parameters upon the squeal. The parameters in the range of $\pm 20\%$ variation and the coefficient of friction of 0·37 were used in the calculation.

It is examined from Figure 10(a) that the positive real parts increase with the parameters in the range from zero to $+20\%$ variation, while they are all zeros in the range of the parameters from zero to -20% variation. This means that A_d and rI should be decreased to reduce the instability of the brake system. On the contrary, Figure 10(b) shows that EI_d, rA and E_{lin} should be increased to reduce the instability. In other words, the increase of the cross-sectional area and the decrease of the bending stiffness of the shoe are advantageous to the reduction of the squeal, and the drum produces the opposite results. Figure 11 shows the influences of the geometric parameters upon the squeal. As shown in this figure, the increase of β_1 and the decrease of β_2 can reduce the squeal, and γ_1 and γ_2 also have the same effects respectively. The angular distance δ has an optimum value close to the original value which has no variation. The influences of these parameters upon the squeal can vary with the kind of drum brake and the frequency of the squeal.

It is generally accepted that the wave motion easily occurs in axisymmetric structures, and is oppressed by adding asymmetry. The lumped masses were attached to the drum for the asymmetry, and the influences of the masses were analyzed with the coefficient of friction of 1·0 which is much higher than that of the critical value. The system is extremely unstable when the value of the coefficient of friction is much higher than the critical value. The added masses were equally spaced on the circumference to keep the balance of the drum. It is seen from Figure 12 that the 2 and the 3 added masses are effective to the squeal while the 4 masses are not. This is because the 2 and the 3 split up the natural frequency of the ring's pair mode into the two very different frequencies, as compared with the 4. As shown in Figure 8(a), the larger the difference between the two frequencies, the higher the value of the critical coefficient of friction.

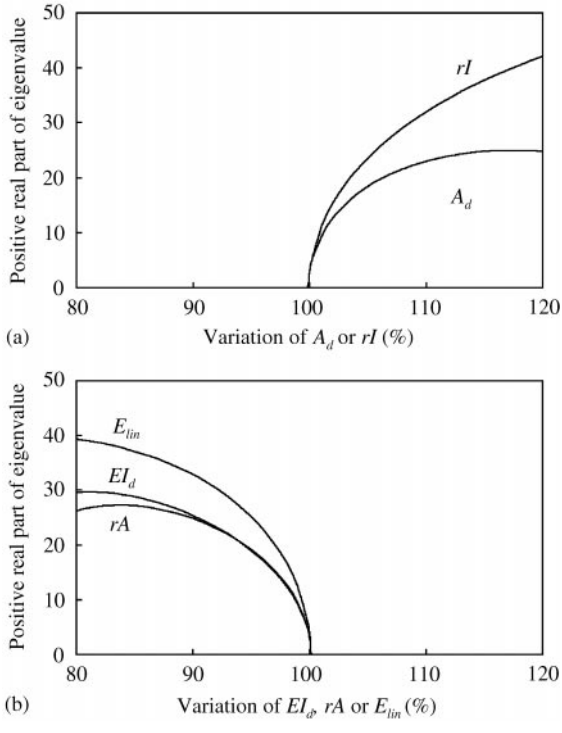

Figure 10. Positive real parts of the eigenvalues with variations of (a) A_d, rI and (b) EI_d, rA, E_{lin}.

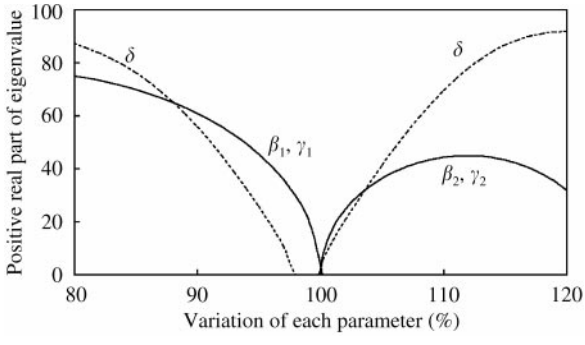

Figure 11. Positive real parts of the eigenvalues with variations of the assemble angles.

6.3. MODIFICATION OF THE PARTIAL SHAPE OF THE WEB

The parameter studies has brought up the fact that the squeal is reduced by the increase of the cross-sectional area and the decrease of the bending stiffness of the shoe. However, the two modifications of the shoe cannot be carried out simultaneously. Accordingly, the bending stiffness should be decreased effectively with minimum decrease in the cross-sectional area.

To carry out this process, the small parts at which the strain was concentrated were modified as little as possible. The concentrated strain was found from the strain energy distribution of the shoe obtained by FEM; Figure 13 shows the strain energy distribution of mode No. 2s of the shoe. Figure 14 shows the profile of the web modified by cutting the

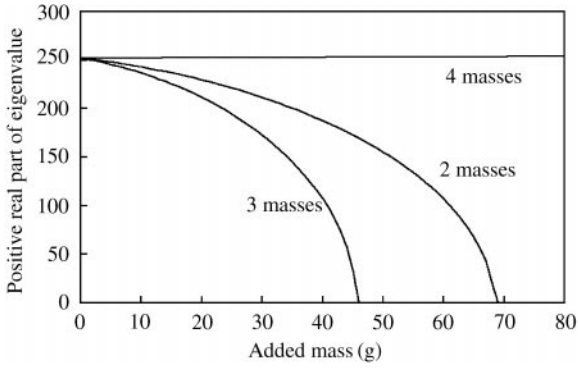

Figure 12. Positive real parts of the eigenvalues with variations of the added masses.

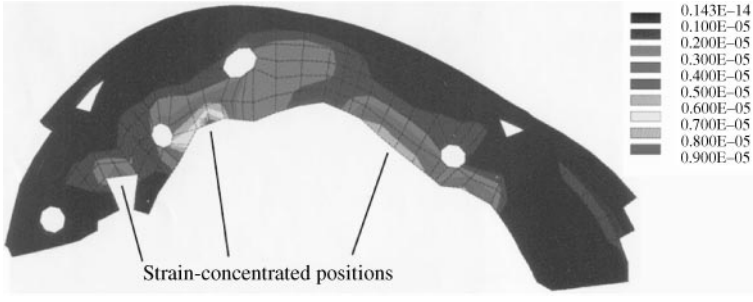

Figure 13. Strain energy distribution of mode No. 2s of the shoe extracted from the FE analysis.

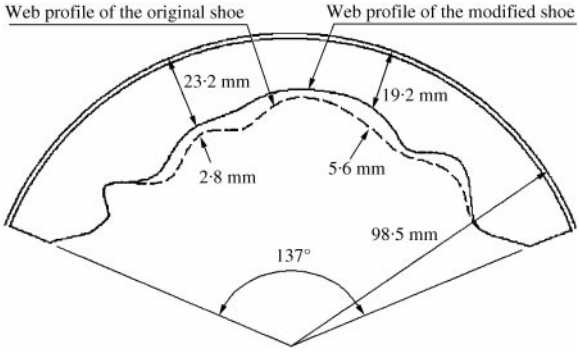

Figure 14. Web profile of the original and the modified shoe obtained by spline functions.

several parts, and also Table 4 shows the natural frequencies of the shoe and the critical coefficients of friction calculated in the analysis before and after the modification. The increase in the critical coefficient of friction means that the squeal would be reduced by that modification.

6.4. VERIFICATION THROUGH NOISE DYNAMOMETER TESTS

The effect of the modification of the web has been verified through noise dynamometer tests shown in Figure 15. The drum brake was combined with the rear wheel, and the

TABLE 4

Natural frequencies of the shoe and critical coefficients of friction before and after modification

	Natural frequency of second bending mode (kHz)	Critical coefficient of friction
Original shoe	5·56	0·37
Modified shoe	4·78	0·54
Ratio	−14·0%	+45%

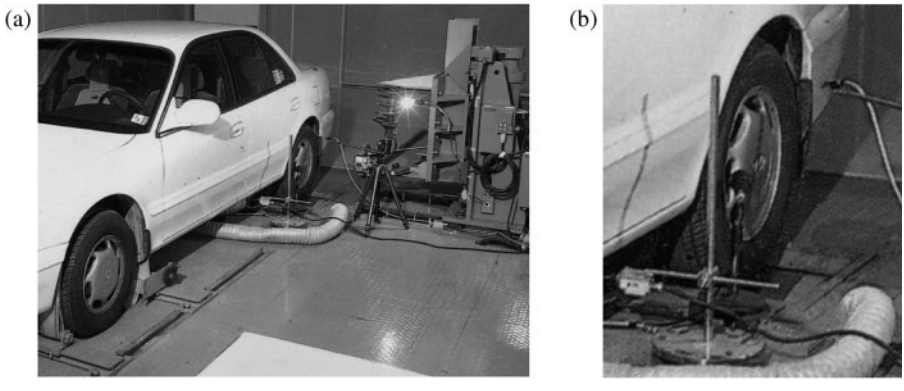

Figure 15. Photo of (a) the noise dynamometer test and (b) enlarged photo of the rear wheel with which the drum brake is combined.

TABLE 5

Result of noise dynamometer tests

Test no.	Type of shoe	Noise ratio (%)	Noise index	Remarks
1	Original shoe	0·25	0·31	Not exceeded noise limit (squeal occurred)
2	Original shoe	0·23	4·00	Exceeded noise limit
3	Modified shoe	0·00	0·00	No squeal occurred
4	Modified shoe	0·00	0·00	No squeal occurred

number of times and the sound pressure levels of the squeal were measured by a microphone. From these measured data, noise ratios and noise indexes were calculated and these values are represented in Table 5 compared with the noise limit demanded by buyers.

Noise ratio is a ratio of the number of squeal occurrence to the total number of braking, and noise index is a value obtained by non-dimensionalizing the sound pressure of the squeal occurred. Therefore, the bigger the noise ratio, the more the squeal occurrence, and the bigger the noise index, the louder the sound of squeal. Four tests were performed, and the total number of braking was 3543 per a test; it took 5 days to finish 1 test.

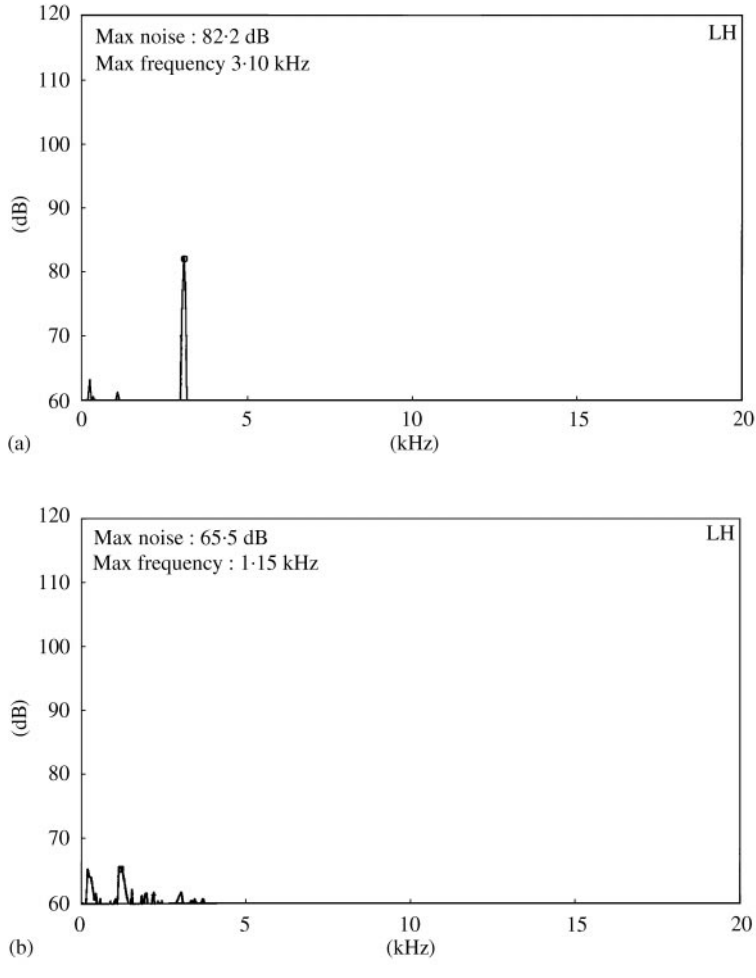

Figure 16. Spectrums of the drum brake noise measured in the noise dynamometer test: (a) the original shoe used and 3·1 kHz squeal occurred; (b) the modified shoe used and no squeal occurred.

It is found from Table 5 that the drum brake with the modified shoe generates no squeal contrary to the original shoe. Figure 16 shows the sound spectrums of the brake with the original or the modified shoe; the other spectral lines except the dominant peak of 3·1 kHz in Figure 16 are environmental noises. From the above results, the partial modification of the web is found to be effective in reducing the squeal occurrence.

7. CONCLUSIONS

In this paper, a theoretical analysis was carried out to reduce the squeal of a drum brake which has shoes of *non-uniform cross-section*, and the influences of the brake design parameters upon the squeal were investigated.

All the results show that the squeal would be reduced by changing the dynamic characteristics of the brake components. In the case of the shoe, the increase of the cross-sectional area and the decrease of the bending stiffness reduce the squeal of the drum

brake. However, they cannot be performed simultaneously, so a method of modification was proposed to effectively reduce the bending stiffness of the shoe with the minimum decrease of the cross-sectional area by considering the strain energy distribution. According to this method, a minor change of the cross-section was performed, and the effect of the change was confirmed through the theoretical analysis and the noise dynamometer tests. As a result, it has been concluded that even a minor change of the shoe has a great effect on the reduction of the squeal.

Finally, the effects of the asymmetry of the drum were also investigated considering the relation between the instability and the wave motion.

REFERENCES

1. C. M. KOOTWIJK-DAMMAN 1996 *Journal of Sound and Vibration* **193**, 451–452. Industrial noise in railway yards; the problem of squeal noise.
2. M. NAKAI and S. AKIYAMA 1998 *Journal of Vibration and Acoustics-Transactions of the ASME* **120**, 614–622. Railway wheel squeal (squeal of disk subjected to periodic excitation).
3. A. J. MCMILLAN 1997 *Journal of Sound and Vibration* **205**, 323–335. A non-linear friction model for self-excited vibrations.
4. D. SINCLAIR 1955 *Journal of Applied Mechanics* **22**, 207–214. Frictional vibrations.
5. P. R. BASFORD and S. B. TWISS 1958 *Transactions of the ASME* **80**, 402–406. Properties of friction materials I—experiments on variables affecting noise.
6. P. R. BASFORD and S. B. TWISS 1958 *Transactions of the ASME* **80**, 407–410. Properties of friction materials II—theory of vibrations in brakes.
7. R. A. C. FOSBERRY and Z. HOLUBECKI 1955 *Motor Industry Research Association* (*MIRA*) *Research Report* 1955/2. An investigation of the cause and nature of brake squeal.
8. R. A. C. FOSBERRY and Z. HOLUBECKI 1957 *Motor Industry Research Association* (*MIRA*) *Research Report* 1957/3. Third report on squeal of drum brakes.
9. N. MILLNER 1976 *Institute of Mechanical Engineers paper* C39/76, pp. 177–185. A theory of drum brake squeal.
10. H. OKAMURA and M. NISHIWAKI 1989 *JSME International Series* III **32**, 206–214. A study on brake noise-drum brake squeal.
11. A. M. LANG and T. P. NEWCOMB 1990 *SAE paper* 905170. The vibration characteristics of squealing brakes.
12. S. CHEN and D. GUAN 1991 *SAE paper* 912497, pp. 371–375. Theoretical and experimental study on drum brake squeal.
13. X. ZHU and D. GUAN 1993 *SAE paper* 931879. The experimental and simulational analysis on drum brake squeal by structurally closed-loop coupling model.
14. J. HULTEN 1995 *SAE paper* 932965. Drum brake squeal—a self-exciting mechanism with constant friction.
15. J. HULTEN 1995 *SAE paper* 951280. pp. 377–388. Some drum brake squeal mechanisms.
16. J. HULTEN 1997 *Proceedings of the* 1997 *ASME Design Engineering Technical Conferences* DETC97/VIB-4161. Friction phenomena related to drum brake squeal instabilities.
17. J. HULTEN, J. FLINT and T. NELLEMOSE 1997 *SAE paper* 972028. Mode shape of a squealing drum brake.
18. A. M. LANG, D. R. SCHAFER, T. P. NEWCOMB and P. C. BROOKS 1993 *Institute of Mechanical Engineers paper* C444/016/93. pp. 161–171. Brake squeal—the influence of rotor geometry.

APPENDIX A

$$c_1 = \pi\rho_d A_d r_d(n^2+1) + \sum_{k=1}^{r} m_k\{(n^2-1)\sin^2(n\theta_k)+1\},$$

$$c_2 = \pi\rho_d A_d r_d(n^2+1) + \sum_{k=1}^{r} m_k\{(n^2-1)\cos^2(n\theta_k)+1\},$$

$$c_3 = -\sum_{k=1}^{r} m_k(n^2-1)\sin(n\theta_k)\cos(n\theta_k), \qquad c_4 = \pi n^2(n^2-1)^2\frac{EI_d}{r_d^3},$$

$$c_5 = \int_{-\beta_1}^{\beta_2} \sin^2(n\theta)\,\mathrm{d}\theta + \int_{-\gamma_1}^{\gamma_2} \sin^2\{n(\phi+\delta)\}\,\mathrm{d}\phi,$$

$$c_6 = \int_{-\beta_1}^{\beta_2} \sin(2n\theta)\,\mathrm{d}\theta + \int_{-\gamma_1}^{\gamma_2} \sin\{2n(\phi+\delta)\}\,\mathrm{d}\phi,$$

$$c_7 = \int_{-\beta_1}^{\beta_2} \cos^2(n\theta)\,\mathrm{d}\theta + \int_{-\gamma_1}^{\gamma_2} \cos^2\{n(\phi+\delta)\}\,\mathrm{d}\phi,$$

$$c_{8i} = \int_{-\beta_1}^{\beta_2} \theta^{i-1}\sin(n\theta)\,\mathrm{d}\theta, \qquad c_{8j} = \int_{-\beta_1}^{\beta_2} \theta^{j-1}\sin(n\theta)\,\mathrm{d}\theta,$$

$$c_{9i} = \int_{-\beta_1}^{\beta_2} \theta^{i-1}\cos(n\theta)\,\mathrm{d}\theta, \qquad c_{9j} = \int_{-\beta_1}^{\beta_2} \theta^{j-1}\cos(n\theta)\,\mathrm{d}\theta,$$

$$c_{10i} = \int_{-\gamma_1}^{\gamma_2} \phi^{i-1}\sin\{n(\phi+\delta)\}\,\mathrm{d}\phi, \qquad c_{10j} = \int_{-\gamma_1}^{\gamma_2} \phi^{j-1}\sin\{n(\phi+\delta)\}\,\mathrm{d}\phi,$$

$$c_{11i} = \int_{-\gamma_1}^{\gamma_2} \phi^{i-1}\cos\{n(\phi+\delta)\}\,\mathrm{d}\phi, \qquad c_{11j} = \int_{-\gamma_1}^{\gamma_2} \phi^{j-1}\cos\{n(\phi+\delta)\}\,\mathrm{d}\phi,$$

$$c_{12} = \rho_1\int_{-\alpha}^{\alpha} A_1 r_1\theta^{i+j-2}\,\mathrm{d}\theta, \qquad c_{13} = \rho_2\int_{-\alpha}^{\alpha} A_2 r_2\phi^{i+j-2}\,\mathrm{d}\phi,$$

$$c_{14} = E_1\int_{-\alpha}^{\alpha}\left\{-\frac{I_1}{r_1^3}(i-1)(j-1)(j-2)\theta^{i+j-5} + \frac{A_1}{r_1}(i-1)\theta^{i+j-3}\right\}\mathrm{d}\theta,$$

$$c_{15} = E_2\int_{-\alpha}^{\alpha}\left\{-\frac{I_2}{r_2^3}(i-1)(j-1)(j-2)\phi^{i+j-5} + \frac{A_2}{r_2}(i-1)\phi^{i+j-3}\right\}\mathrm{d}\phi,$$

$$c_{16} = E_1\int_{-\alpha}^{\alpha}\left\{-\frac{I_1}{r_1^3}(i-1)(i-2)(j-1)\theta^{i+j-5} + \frac{A_1}{r_1}(j-1)\theta^{i+j-3}\right\}\mathrm{d}\theta,$$

$$c_{17} = E_2\int_{-\alpha}^{\alpha}\left\{-\frac{I_2}{r_2^3}(i-1)(i-2)(j-1)\phi^{i+j-5} + \frac{A_2}{r_2}(j-1)\phi^{i+j-3}\right\}\mathrm{d}\phi,$$

$$c_{18} = E_1\int_{-\alpha}^{\alpha}\left\{\frac{I_1}{r_1^3}(i-1)(i-2)(j-1)(j-2)\theta^{i+j-6} + \frac{A_1}{r_1}\theta^{i+j-2}\right\}\mathrm{d}\theta,$$

$$c_{19} = E_2\int_{-\alpha}^{\alpha}\left\{\frac{I_2}{r_2^3}(i-1)(i-2)(j-1)(j-2)\phi^{i+j-6} + \frac{A_2}{r_2}\phi^{i+j-2}\right\}\mathrm{d}\phi,$$

$$c_{20} = E_1\int_{-\alpha}^{\alpha}\left\{+\frac{I_1}{r_1^3}(i-1)(j-1)\theta^{i+j-4} + \frac{A_1}{r_1}(i-1)(j-1)\theta^{i+j-4}\right\}\mathrm{d}\theta,$$

$$c_{21} = E_2\int_{-\alpha}^{\alpha}\left\{+\frac{I_2}{r_2^3}(i-1)(j-1)\theta^{i+j-4} + \frac{A_2}{r_2}(i-1)(j-1)\phi^{i+j-4}\right\}\mathrm{d}\phi,$$

$$c_{22} = \int_{-\beta_1}^{\beta_2} \theta^{i+j-2}\,\mathrm{d}\theta, \qquad c_{23} = \int_{-\gamma_1}^{\gamma_2} \phi^{i+j-2}\,\mathrm{d}\phi,$$

$$c_{24} = k_2 \sin\{2(\alpha-\varepsilon)\}(-\alpha)^{i+j-2} - k_1 \sin\{2(\alpha+\varepsilon)\}\alpha^{i+j-2},$$

$$c_{25} = k_3 \sin\{2(\alpha+\varepsilon)\}(-\alpha)^{i+j-2} - k_4 \sin\{2(\alpha-\varepsilon)\}\alpha^{i+j-2},$$

$$c_{26} = k_2 \sin^2(\alpha-\varepsilon)(-\alpha)^{i+j-2} + k_1 \sin^2(\alpha+\varepsilon)\alpha^{i+j-2},$$

$$c_{27} = k_3 \sin^2(\alpha+\varepsilon)(-\alpha)^{i+j-2} + k_4 \sin^2(\alpha-\varepsilon)\alpha^{i+j-2},$$

$$c_{28} = k_2 \cos^2(\alpha-\varepsilon)(-\alpha)^{i+j-2} + k_1 \cos^2(\alpha+\varepsilon)\alpha^{i+j-2},$$

$$c_{29} = k_3 \cos^2(\alpha+\varepsilon)(-\alpha)^{i+j-2} + k_4 \cos^2(\alpha-\varepsilon)\alpha^{i+j-2}.$$

APPENDIX B

$$\mathbf{M}_{11}(1,1) = c_1, \qquad \mathbf{M}_{11}(2,2) = c_2, \qquad \mathbf{M}_{11}(1,2) = \mathbf{M}_{11}(2,1) = c_3,$$

$$\mathbf{M}_{22}(i,j) = \mathbf{M}_{33}(i,j) = c_{12}, \qquad \mathbf{M}_{44}(i,j) = \mathbf{M}_{55}(i,j) = c_{13},$$

$$\mathbf{K}_{11}(1,1) = c_4 + k_{lin}n^2c_5 + 0{\cdot}5\mu k_{lin}nc_6, \qquad \mathbf{K}_{11}(1,2) = -0{\cdot}5k_{lin}n^2c_6 - \mu k_{lin}nc_7,$$

$$\mathbf{K}_{11}(2,1) = -0{\cdot}5k_{lin}n^2c_6 + \mu k_{lin}nc_5, \qquad \mathbf{K}_{11}(2,2) = c_4 + k_{lin}n^2c_7 - 0{\cdot}5\mu k_{lin}nc_6,$$

$$\mathbf{K}_{12}(1,j) = -k_{lin}nc_{8j} - \mu k_{lin}c_{9j}, \qquad \mathbf{K}_{12}(2,j) = k_{lin}nc_{9j} - \mu k_{lin}c_{8j},$$

$$\mathbf{K}_{14}(1,j) = -k_{lin}nc_{10j} - \mu k_{lin}c_{11j}, \qquad \mathbf{K}_{14}(2,j) = k_{lin}nc_{11j} - \mu k_{lin}c_{10j},$$

$$\mathbf{K}_{21}(i,1) = -k_{lin}nc_{8i}, \qquad \mathbf{K}_{21}(i,2) = k_{lin}nc_{9i},$$

$$\mathbf{K}_{22}(i,j) = c_{18} + k_{lin}c_{22} + c_{28}, \qquad \mathbf{K}_{23}(i,j) = c_{16} + 0{\cdot}5c_{24},$$

$$\mathbf{K}_{31}(i,1) = -\mu k_{lin}nc_{8i}, \qquad \mathbf{K}_{31}(i,2) = \mu k_{lin}nc_{9i},$$

$$\mathbf{K}_{32}(i,j) = c_{14} + 0{\cdot}5c_{24} + \mu k_{lin}c_{22}, \qquad \mathbf{K}_{33}(i,j) = c_{20} + c_{26},$$

$$\mathbf{K}_{41}(i,1) = -k_{lin}nc_{10i}, \qquad \mathbf{K}_{41}(i,2) = k_{lin}nc_{11i},$$

$$\mathbf{K}_{44}(i,j) = c_{19} + k_{lin}c_{23} + c_{29}, \qquad \mathbf{K}_{45}(i,j) = c_{17} + 0{\cdot}5c_{25},$$

$$\mathbf{K}_{51}(i,1) = -\mu k_{lin}nc_{10i}, \qquad \mathbf{K}_{51}(i,2) = \mu k_{lin}nc_{11i},$$

$$\mathbf{K}_{54}(i,j) = c_{15} + 0{\cdot}5c_{25} + \mu k_{lin}c_{23}, \qquad \mathbf{K}_{55}(i,j) = c_{21} + c_{27},$$

$$(i = 1\text{–}N,\ j = 1\text{–}N).$$

All other components are zero.